Photo-induced Properties of Non-annealed Anatase TiO_2 Mesoporous Film Prepared by Anodizing in the Hot Phosphate/glycerol Electrolyte

Yoshiaki Taguchi[1], *Etsushi Tsuji*[2,*], *Yoshitaka Aoki*[2], *Hiroki Habazaki*[2]

[1]Graduate School of Chemical Sciences and Engineering, [2]Division of Materials Chemistry, Faculty of Engineering, Hokkaido University, Sapporo, Hokkaido, 060-8628, Japan

Corresponding author: Phone & Fax: +81-11-706-6736, e-mail: e-tsuji@eng.hokudai.ac.jp

ABSTRACT

In this study, anatase crystalline TiO_2 mesoporous films were ~~was~~ formed by anodizing of titanium specimens without annealing procedures. The specimens were anodized at 3 and 20 V in 0.6 mol dm^{-3} K_2HPO_4 and 0.2 mol dm^{-3} K_3PO_4/glycerol electrolyte at 433 K. The obtained films had mesoporous structures with pore diameters as small as ~10 nm. The mesoporous film formed at 20 V without annealing (MP-20V) was a mixture of amorphous phase and nanograined anatase, which clearly showed strong <001> preferred orientation, whereas that at 3 V was completely amorphous. Even without annealing, the MP-20V showed high photocatalytic activities for decomposition of water and methylene blue. In contrast, the anodic TiO_2 nanotube film formed in NH_4F/ethylene glycol electrolyte revealed photocatalytic activities only after annealing at 723 K, because of the amorphous nature of the as-anodized nanotube film. The MP-20V film also showed superhydrophilicity with UV light irradiation.

1. Introduction

TiO_2 is one of the most famous photocatalysts and widely used for various applications such as photodecomposition techniques of water [1,2] and organic compounds [3,4], antifog materials [5], dye-sensitized solar cells (DSSC) [6-8] and so on. In general, amorphous semiconductors have a lot of defects which often act as recombination centers of photogenerated carries [9,10]. Thus, it is quite important to prepare highly crystalline TiO_2 films. In addition, a high surface area of TiO_2 is necessary for photocatalysts and DSSCs. TiO_2 nanoparticles films are often formed by spin-coating, doctor-blading and sputtering methods. Recently, TiO_2 nanotubular and nanoporous films prepared by anodizing of titanium specimens have much attention due to such unique structures, high surface area [11,12] and superior electron transport to that of TiO_2 nanoparticle films [13,14]. The TiO_2 nanotubular films have been formed by anodizing in organic electrolytes containing fluoride ions [11-14]. However, such anodic TiO_2 nanotubular films are highly contaminated with fluoride and carbon species derived from the electrolyte, leading to amorphous structures. Therefore, post-annealing of the anodized specimens at elevated temperatures is indispensable for removing such impurities and crystallization of TiO_2 nanotubes. If crystalline TiO_2 nanoporous films are prepared without annealing procedures, some heat-labile materials such as plastic sheets and ITO conducting glass can be used as new substrates.

More recently, in our previous report, titanium has been anodized in a hot glycerol electrolyte containing K_3PO_4 and K_2HPO_4 with reduced water content to grow relatively thick anodic TiO_2 mesoporous films [15]. The pore diameters of the obtained TiO_2 mesoporous films were in the range of 6 - 16 nm which were smaller than those of TiO_2 nanotubes formed in organic electrolytes containing fluoride ions, leading to much large available surface area. In addition, the TiO_2 mesoporous film contained only small amounts of impurities such as phosphate and was already crystallized to anatase structure just after anodizing at 20 V. The similar results were reported by other researchers [16-19]. Schmuki et al. reported that the self-organized TiO_2 nanostructures such as nanotube, mesoporous, channel and fishbone structures were formed by anodizing in a hot glycerol containing only K_2HPO_4 at several voltages [17]. They also reported that the obtained TiO_2 nanostructured films after annealing showed good performance for photodecomposition of organic compounds [18] and DSSCs [19]. However, there is no report on photocatalytic and photo-induced properties of the anodic TiO_2 mesoporous films without annealing procedures.

In this study, commercially pure titanium specimens were anodized in K_2HPO_4 and K_3PO_4/glycerol at 433 K, leading to formation of anatase crystalline TiO_2 mesoporous film without annealing procedures. We revealed that the obtained TiO_2 mesoporous film shows high photocatalytic activity for decomposition of water and organic compounds and photo-induced hydrophilicity.

2. Experimental

The specimens used for anodizing were 99.5% pure titanium sheets of 0.5 mm thickness. Prior to anodizing, the specimens were electropolished in 1 mol dm^{-3} NaCl/ethylene glycol solution at 293 K at 20 V for 200 s and subsequently at 10 V for 600 s [20]. A titanium sheet was used as a counter electrode. Then, the electropolished specimens were anodized at 3 and 20 V in a stirred glycerol electrolyte containing 0.6 mol dm^{-3} K_2HPO_4 and 0.2 mol dm^{-3} K_3PO_4 at 433 K under a nitrogen atmosphere. The water content in the electrolyte was ~0.03 mass%. A platinum sheet was used as a counter electrode. The films anodized at 3 and 20 V are denoted as MP-3V and MP-20V, respectively. For comparison, the electropolished titanium specimen was also anodized in 0.25 wt% NH_4F and 1vol% water/ethylene glycol electrolyte at 60 V (denoted as NT) [21]. For evaluation of the effective surface area, the depth profile, photocatalytic activity and photo-induced hydrophilicity of the anodic films, the films of ~ 5 μm thickness were used.

Surface and cross-section morphologies of the anodized specimens were observed using a scanning electron microscope (SEM) (JEOL, JSM-6500F) operated at 10 kV. Further, selected specimens were examined in a transmission electron microscope (TEM) (JEOL, JEM-2000FX) operated at 200 kV. Electron transparent sections, ~20 nm thick, were obtained using ultramicrotomy. Depth profiles of the anodized specimens were obtained by a glow discharge optical emission spectroscopy (GDOES) (Jobin-Yvon 5000 RF) in an argon

atmosphere of 600 Pa with application of RF of 13.56 MHz and power of 50 W. Light emissions of characteristic wavelengths were monitored throughout the analysis with a sampling time of 0.01 s to obtain depth profiles. The wavelengths of the spectral lines used were 365.350, 178.287, 130.217 and 165.701 nm for titanium, phosphorus, oxygen and carbon respectively. The signals were detected from a circular area of approximately 4 mm diameter. The chemical composition of the obtained films was also examined using energy dispersive X-ray spectroscopy (EDS) facilities equipped the SEM. In order to estimate the pore size and the effective surface areas in the anodic films, nitrogen gas adsorption/desorption isotherms (Bel Japan, Belsorp-max instrument) were measured at 77 K. The pore size distribution was analyzed using BJH method [22], which is useful for mesopores in the range of 2–50 nm size. The structure of the anodic films was identified by X-ray diffraction (XRD) (Rigaku, RINT-2000) using Cu Kα radiation.

The current density (*j*) vs potential (*E*) curves of the anodized specimens for oxygen photoevolution were measured by using a normal three-electrode system. A platinum sheet and an Ag/AgCl/KCl(satd) electrode were used as a counter electrode and a reference electrode, respectively. The working electrodes were prepared by attaching an aluminum wire on the edge of the specimens with silver paste, followed by covering the surface with epoxy resin for insulation, except for an area of 1.0 × 1.0 cm^2 in the center (all the current densities were calculated by using these geometrical surface areas). The electrodes were mounted in an

electrochemical cell having a quartz window, and UV irradiation was carried out by the 365 nm band from a 500 W high-pressure xenon lamp(WACOM, HX-504), obtained by using of 33U band-pass filter (ASAHI SPECTRA,UTVAF 50S-33U). The electrochemical measurements were carried out using commercial potentiostat (Princeton Applied Research, EG&G 263A) and potential programmer (Princeton Applied Research, Electrochemistry Power Suite). The intensity of the UV light was 60 mW/cm^2 which was measured with a thermopile (NEO ARK, PM-335A). The electrolyte used for photo-induced water decomposition was deoxygenated 0.1 M $HClO_4$ aqueous solution (pH 1.3). Applied potential was swept from -0.5 to 1.5 V vs Ag/AgCl/KCl(satd) with a potential-sweep rate of 50 mV s^{-1}. In all of the experiments, special-grade chemicals were used without further purification. Deionized water purified with a Milli-Q water purification system was used in the present study.

Photocatalytic activity for decomposition of an organic compound was evaluated on the basis of the decomposition of methylene blue (MB) in an aqueous solution. 10×10^{-5} mol dm^{-3} MB aqueous solution was prepared and the anodized specimens were sintered in it. After stirring for 15 min without UV irradiation to reach the adsorption equilibrium, the anodized specimens were irradiated with UV light under the same condition as the *j* - *E* measurements and the 2 mL of the MB solution was collected every half hour. The photocatalytic activity was examined by monitoring the reduction of the absorbance at 665 nm. The

spectrophotometric measurements were carried out using a UV/Vis spectrometer (JASCO Corp., JASCO V-550).

The wettability of the obtained specimens was evaluated by contact angle measurements for liquid droplets (2 μL) of water (Kyowa Interface Science Co., DM-CE1). UV irradiation was carried out by the 365 nm band using handy UV lamp (AS ONE, SLUV-8) for several hours.

3. Results and discussion

Fig. 1 shows the current transients of titanium during anodizing in hot phosphate/glycerol electrolytes containing 0.03% water at formation voltages of 3 and 20 V for 3.6 ks (MP-3V and MP-20V). In our previous report [15], thick anodic titanium oxide films can be formed on commercially pure titanium in the electrolyte containing little water. In this condition, the formation voltages of 3 or 20 V are rapidly attained during the initial period of anodizing. The initial current density at 20 V was larger than that at 3 V. Then, the current density decreases with anodizing time and the final current densities at both formation voltages were almost the same. The gradual current decrease in the anodic films with anodizing time are typical in the hot phosphate/glycerol electrolyte [23-26] , although porous anodic alumina films formed in aqueous acid electrolytes show a steady-state current density [27].

Fig. 2 shows cross-sectional SEM observations of the (a) MP-3V and (b) MP-20V formed for 3.6 ks. From the inset images in Fig.2, the thickness of the MP-3V and MP-20V are 13.8 and 5.7 μm, whereas the current density of the later one during anodizing was higher than that of the former one. This is because the MP-20V was crystallized during anodizing (the details of it are described later), leading oxygen evolution at the crystalline grains [28]. The MP-3V film has cylindrical pores, which are normal to the metal/film interface, whereas the MP-20V has rather irregular pores. The formation voltage-dependent pore structures were also reported by other researchers [17], but the detail mechanisms of the mesoporous formation haven't clarified yet. Those films showed good adhesion to the titanium substrates.

Since the pore size was not clearly identified by the SEM observations, the pore size distribution has been examined using nitrogen gas adsorption/desorption isotherms. Each film thickness was 5 μm. Fig. 3 shows the pore size distributions of the MP-3V, MP-20V and the TiO_2 nanotubes anodized in NH_4F/ethylene glycol electrolyte at 60 V (NT) obtained from nitrogen adsorption isotherms. In this figure, V_p and d_p denotes the pore volume and the pore diameter, respectively. The peak pore diameters of the MP-3V and MP-20V are not voltage-dependent, being ~10 nm. The similar result was reported in our previous paper [15]. Table 1 shows the BET roughness factors of the MP-3V and MP-20V together with the NT (5 μm thickness). The BET roughness factors of the MP-3V and MP-20V are 1314 and 650, indicating that those values increased when the formation voltage decreased from 20 to 3 V. In

addition, the BET roughness factors of MP-3V and MP-20V are much larger than that of the NT. The smaller pore sizes and cell sizes of the MP-3V and MP-20V in comparison with those of the NT contribute to the higher roughness factors.

Fig.4 shows GDOES depth profiles of the MP-3V (Fig. 4(a)) and MP-20V (Fig. 4(b)). The films are oxide-based, since the intensity ratio of oxygen to titanium was similar to TiO_2 film formed in an aqueous electrolyte. The oxygen source to form anodic films should be the water impurity in the electrolyte [27]. The films contain carbon species probably derived from ethylene glycol. The phosphorous is incorporated into the anodic films and the incorporation is also dependent upon the formation voltage. The phosphorus content in the MP-20V, examined by EDS, was ~2.1 at.% ([P]/([Ti]+[O]+[P])) while in the MP-3V, <0.5 at.% phosphorus was incorporated. Even in the MP-20V film, the phosphorous content was much lower than the fluorine content in the NT (~16.6 at% ([F]/([Ti]+[O]+[F]))).

Fig.5 shows XRD patterns of the MP-3V and MP-20V, together with the NT annealed at 723 K for 3 h. The XRD pattern of the MP-3V showed only broad diffraction halo between 20 and 30º, apart from the intense substrate peaks, indicating that the MP-3V film was amorphous. In contrast, the sharp peaks due to the presence of anatase crystal appeared in the pattern of the MP-20V, even though the film was not annealed after anodizing. This result suggested that increasing of the formation voltage promoted crystallization of TiO_2 films, whereas it was known that crystallization in the fluoride-containing organic and aqueous

electrolytes was not promoted. It is well known that electric field-induced crystallization of anodic TiO_2 occurs at and above 5 V in aqueous electrolytes at ambient temperatures [28]. Similarly, the crystallization of anodic films on titanium appears to occur in the present organic electrolyte at an elevated temperature, when the formation voltage exceeds at ~5 V.

Another remarkable feature of the MP-20V specimen is that the 004 peak anatase TiO_2 is the strongest, whereas the most intense 101 peak for randomly oriented anatase is missing. Schmuki et al. also reported the formation of {001} oriented anatase nanoporous film in a hot K_2HPO_4/glycerol at 50 V [17]. The results imply that the formation of anatase mesoporous film with {001} preferred orientation is characteristic of the hot phosphate/glycerol electrolytes.

More detail structure of the MP-20V anodic film was examined by high resolution TEM (Fig. 6). Fig. 6 shows TEM images (Fig. 6 (a-b)) and the diffraction pattern (Fig. 6(c)) of the MP-20V, respectively. Fig. 6(a) discloses from the diffraction contrasts that the anodic film on titanium, which appears at the bottom of the micrograph, contained nanocrystals. From Fig. 6 (b), it is obvious that the nanocrystals are surrounded by amorphous matrix. The spacing of the lattice fringes in the nanocrystals is 0.35 nm, corresponding to the spacing of (101) face of anatase. The size of nanocrystals is ~ 10 - 20 nm (see the areas circled by white lines in Fig. 6 (b)). A selected area diffraction pattern, shown in Fig. 6(c), also reveals that the {001} face of anatase is coincidence with the growth direction of the anodic film.

Fig. 7 shows *j-E* curves of the MP-3V without and with UV light irradiation, the MP-20V with UV light irradiation, together with that of the NT annealed at 723 K with UV light irradiation. All the anodic films used in this study were of ~ 5 μm thickness. In the case of the MP-3V, photocurrent was extremely small, indicating that photocatalytic activity for oxygen photoevolution was very low. This low activity for oxygen photoevolution may be caused by low crystallinity, because it is well known that amorphous structure has a lot of defects which act as the recombination centers of photogenerated carriers [9,10]. On the other hand, in the case of the MP-20V, the TiO_2 mesoporous film shows good performance even without post-annealing. The saturated photocurrent density of the MP-20V is as high as that of the annealed NT. The high photocatalytic activity of the MP-20V must be induced by anatase crystalline nanocrystals contained in the film. In addition, Miraghaei et al. reported that good adhesion of the anodic TiO_2 nanotubular films to the substrates improved the photoelectrochemical properties [29,30]. Therefore, the good adhesion of the MP-20V to the titanium substrates may also improve the photoelectorchemical performance.

The similar result was also obtained in photodecomposition of the organic compound. Fig. 8 shows the comparison of photocatalytic decomposition rates of MB for the MP-3V, MP-20V and NT annealed at 723 K. Assuming the first-order decomposition kinetics[31,32], $\ln(C/C_0)$ is plotted as a function of photo-irradiation time, t. The rate of decomposition of MB on the MP-20V was much faster than that on the MP-3V due to the difference of crystallinity.

The photocatalytic activity of the MP-20V for MB decomposition was also as high as that of NT after annealing.

Fig. 9 shows the static contact angles of the MP-3V, MP-20V and NT surface for water. The water contact angles of both the MP-3V and MP-20V decreased to steady values within UV irradiation for 1 h. We can see that the contact angle of the MP-20V after UV irradiation was ~8º, whereas that of MP-3V was ~16º. Surfaces with a contact angle of less than 10º are called superhydrophilic [33], such that the MP-20V shows superhydrophilicity after UV irradiation. However, both film surfaces after UV irradiation show the contact angles higher than the surface of the UV-irradiated NT. Such difference may be caused by the difference of surface roughness and/or crystallinity of the TiO_2 films. As shown in Table 1, the BET roughness factors of MP-3V and MP-20V are much larger than that of NT. It is well known that the surface roughness emphasizes the wettability in accord with the Wenzel model [33-35]. The model suggests that the contact angle of the rough hydrophilic surface such as TiO_2 is smaller than that of smooth surface. Therefore, from points of view of the surface roughness, the contact angles of MP-3V and MP-20V are expected to be smaller than that of NT. On the other hand, as already mentioned in XRD and TEM results, we can see that the MP-3V was amorphous and the MP-20V was mixture of amorphous and anatase crystalline grains. There are a lot of reports on the photo-induced superhydrophilicity of TiO_2 [36-39]. Masahashi et al. studied the superhydrophilicity of TiO_2 films formed by anodizing in a

sulfuric acid electrolyte [36]. They reported that the water contact angle of the as-anodized film decreased with the formation voltage, whereas the anatase crystalline film after annealing exhibited further reduced contact angle. The O 1s XPS spectra of the films have a shoulder peak due to adsorption of hydroxyl groups and the intensity of the peak increases with annealing, suggesting that the surface of the annealed film interacts strongly with the hydroxyl groups. Therefore, they concluded that the enhancement in superhydrophilicity is closely related to the formation of highly crystallized anatase TiO_2, which is obtained by increasing the formation voltage or the subsequent annealing. As mentioned above, in this study, the contact angle of NT after UV irradiation was smaller than those of MP-3V and MP-20V, even though the roughness factors of MP-3V and MP-20V were much larger than that of NT. Therefore, this result implies that the contact angle of these specimens after UV irradiation is mainly affected by the difference of crystallinity rather than that of surface roughness.

4. Conclusions

The TiO_2 mesoporous film can be formed by anodizing of titanium specimens in the hot phosphate/glycerol electrolyte. Anatase phase with {001} preferred orientation to the direction of film growth is developed by anodizing at 20 V without post-annealing. The film formed at 20 V contains phosphate species incorporated from electrolyte, being probably

mainly incorporated in an amorphous matrix surrounding anatase nanocrystals. The as-anodized anatase TiO_2 mesoporous film shows high photocatalytic activities for decomposition of water and methylene blue and superhydrophilicity.

ACKNOWLEDGMENT

Thanks are due to Professor Shin Mukai, Faculty of Engineering, Hokkaido University, for helping the nitrogen gas adsorption/desorption measurements. The present work was supported by the Global COE Program (Project No. B01: Catalysis as the Basis for Innovation in Materials Science) from the Ministry of Education, Culture, Sports, Science and technology, Japan and the A-STEP program from Japan Science and technology Agency.

REFERENCE

[1] A. Fujishima, K Honda, Electrochemical Photolysis of Water at a Semiconductor Electrode, Nature, 238 (1972) 37-38.

[2] G.K. Mor, K. Shankar, M. Paulose, O.K. Varghese, C.A. Grimes, Enhanced Photocleavage of Water Using Titania Nanotube Arrays, Nano Lett., 5 (2005) 191-195.

[3] Z. Liu, X. Zhang, S. Nishimoto, M. Jin, D.A. Tryk, T. Murakami, A. Fujishima, Highly Ordered TiO_2 Nanotube Arrays with Controllable Length for Photoelectrocatalytic Degradation of Phenol, J. Phys. Chem. C, 112 (2008) 253-259.

[4] Z. Liu, X. Zhang, S. Nishimoto, T. Murakami, A. Fujishima, Efficient Photocatalytic Degradation of Gaseous Acetaldehyde by Highly Ordered TiO_2 Nanotube Arrays, Environ. Sci. Technol., 42 (2008) 8547-8551.

[5] R. Wang, K Hashimoto, A. Fujishima, M. Chikuni, E. Kojima, A. Kitamura, M. Shimohigoshi, T. Watanabe, Light-induced amphiphilic surfaces, Nature, 388 (1997) 431-432.

[6] M. Gratzel, Photoelectrochemical cells, Nature 414 (2001) 338-344.

[7] M.D. Wei, Y. Konishi, H.S. Zhou, M. Yanagida, H. Sugihara, H. Arakawa, Highly efficient dye-sensitized solar cells composed of mesoporous titanium dioxide, J. Mater. Chem., 16 (2006) 1287-1293.

[8] O.K. Varghese, M. Paulose, C.A. Grimes, Long Vertically Aligned Titania Nanotubes on Transparent Conductive Oxide for Highly Efficient Solar Cells, Nat. Nanotechnol., 4 (2009) 592-597.

[9] B. Ohtani, Y. Ogawa, S. Nishimoto, Photocatalytic Activity of Amorphous-Anatase Mixture of Titanium(IV) Oxide Particles Suspended in Aqueous Solutions, J. Phys. Chem. B, 101 (1997) 3746-3752.

[10] O. Carp, C.L. Huisman, A. Reller, Photoinduced reactivity of titanium dioxide, Prog. Solid State Chem., 32 (2004) 33-177.

[11] A. Ghicov, P. Schmuki, Self-ordering electrochemistry: a review on growth and functionality of TiO_2 nanotubes and other self-aligned MO_x structures, Chem. Comm., 20 (2009) 2791-2808.

[12] G.K. Mor, O.K. Varghese, M. Paulose, K. Shankar, C. A. Grimes, A review on highly ordered, vertically oriented TiO_2 nanotube arrays: Fabrication, material properties, and solar energy applications, Sol. Energy Mater. Sol., 90 (2006) 2011-2075.

[13] D. Kuang, J. Brillet, P. Chen, M. Takata, S. Uchida, H. Miura, K. Sumioka, S.M. Zakeeruddin, M Gratzel, Application of Highly Ordered TiO_2 Nanotube Arrays in Flexible Dye-Sensitized Solar Cells, ACS Nano, 2 (2008) 113-1116.

[14] K. Zhu, N.R. Neale, A. Miedaner, A.J. Frank, Enhanced Charge-Collection Efficiencies and Light Scattering in Dye-Sensitized Solar Cells Using Oriented TiO_2 Nanotubes Arrays, Nano Lett., 7 (2007) 69-74.

[15] H. Habazaki, M. Teraoka, Y. Aoki, P. Skeldon, G.E. Thompson, Formation of porous anodic titanium oxide films in hot phosphate/glycerol electrolyte, Electrochim. Acta, 55 (2010) 3939-3943.

[16] N.K. Allam, C.A. Grimes, Room Temperature One-Step Polyol Synthesis of Anatase TiO_2 Nanotube Arrays: Photoelectrochemical Properties, Langmuir, 25 (2009) 7234-7240.

[17] K. Lee, D. Kim, P. Schmuki, Highly self-ordered nanochannel TiO_2 structures by anodization in a hot glycerol electrolyte, Chem. Comm., 47 (2011) 5789-5791.

[18] K. Lee, D. Kim, P. Roy, I. Paramasivam, B.I. Birajdar, E. Spiecker, P. Schmuki, Anodic Formation of Thick Anatase TiO_2 Mesosponge Layers for High-Efficiency Photocatalysis, J. Am. Chem. Soc., 132 (2010) 1478-1479.

[19] D. Kim, K. Lee, P. Roy, B.I. Birajdar, E. Spiecker, P. Schmuki, Formation of a Non-Thickness-Limited Titanium Dioxide Mesosponge and its Use in Dye-Sensitized Solar Cells, Angew. Chem. Int. Ed., 48 (2009) 9326-9329.

[20] K. Fushimi, H. Habazaki, Anodic dissolution of titanium in NaCl-containing ethylene glycol, Electrochim. Acta, 53 (2008) 3371-3376.

[21] H.E. Prakasam, K. Shankar, M. Paulose, O.K. Varghese, C. A. Grimes, A New Benchmark for TiO_2 Nanotube Array Growth by Anodization, J. Phys. Chem. C, 111 (2007) 7235-7241.

[22] E.P. Barrett, L.G. Joyner, P.P. Halenda, The Determination of Pore Volume and Area Distributions in Porous Substances. I. Computations from Nitrogen Isotherms Computations from Nitrogen Isotherms, J. Am. Chem. Soc., 73 (1951) 373-380.

[23] H. Habazaki, Y. Oikawa, K. Fushimi, K. Shimizu, S. Nagata, P. Skeldon, G.E. Thompson, Formation of porous anodic films on ti-si alloys in hot phosphate-glycerol electrolyte, Electrochim. Acta, 53 (2007) 1775-1781.

[24] Y. Oikawa, K. Fushimi, Y. Aoki, H. Habazaki, Growth of porous anodic films on niobium in hot phosphate-glycerol electrolyte, ECS Transactions, 16 (2008) 345-351.

[25] S. Yang, Y. Aoki, H. Habazaki, Effect of electrolyte temperature on the formation of self-organized anodic niobium oxide microcones in hot phosphate-glycerol electrolyte, Appl. Surf. Sci., 257 (2011) 8190-8195.

[26] S. Yang, H. Habazaki, T. Fujii, Y. Aoki, P. Skeldon, G.E. Thompson, Control of morphology and surface wettability of anodic niobium oxide microcones formed in hot phosphate-glycerol electrolytes, Electrochim. Acta, 56 (2011) 7446-7453.

[27] H. Habazaki, Y. Oikawa, K. Fushimi, Y. Aoki, K. Shimizu, P. Skeldon, G.E. Thompson, Importance of water content in formation of porous anodic niobium oxide films in hot phosphate–glycerol electrolyte, Electrochim. Acta, 54 (2009) 946-951.

[28] A. Aladjem, Anodic oxidation of titanium and its alloys, J. Mater. Sci., 8 (1973) 688-704.

[29] S. Miraghaei, F. Ashrafizadeh, K. Raeissi, M. Santamaria, and F. Di Quarto, Electrochemical Investigation in Aqueous Solutions on the Adhesion of As-formed Anodic TiO_2 Nanotubes Grown in Organic Solvent, Electrochemical and Solid-State Letters, 14 (2011) K8-K11.

[30] S. Miraghaei, F. Ashrafizadeh, M. Santamaria, F. Di Quarto and K. Shimizu, Influence of Anodic and Thermal Barrier Layers on Physicochemical Behavior of Anodic TiO_2 Nanotubes, J. Electrochem. Soc., 158 (2011) K197-K204.

[31] J. M. Macak, M. Zlamal, J. Krysa, P. Schmuki, Self-Organized TiO_2 Nanotube Layers as Highly Efficient Photocatalysts, small, 3 (2007) 300-304.

[32] Y. Xie, Photoelectrochemical application of nanotubular titania photoanode, Electrochim. Acta, 51 (2006) 3399-3406.

[33] B. Bhushan, Y.C. Jung, Natural and biomimetic artificial surfaces for superhydrophobicity, self-cleaning, low adhesion, and drag reduction, Prog. Mater. Sci., 56 (2011) 1-108.

[34] K. Liu, X. Yao, L. Jiang, Recent developments in bio-inspired special wettability, Chem. Soc. Rev., 39 (2010) 3240-3255.

[35] P. Roach, N.J. Shirtcliffe, M.I. Newton, Progess in superhydrophobic surface development, Soft Matter, 4 (2008) 224-240.

[36] N. Masahashi, S. Semboshi, N. Ohtsu, M. Oku, Microstructure and superhydrophilicity of anodic TiO_2 films on pure titanium, Thin Solid Films, 516 (2008) 7488–7496.

[37] Y. Gao, Y. Masuda, K. Koumoto, Light-Excited Superhydrophilicity of Amorphous TiO_2 Thin Films Deposited in an Aqueous Peroxotitanate Solution, Langmuir, 20 (2004) 3188-3194.

[38] N. Sakai, A. Fujishima, T.Watanabe, K. Hashimoto, Enhancement of the Photoinduced Hydrophilic Conversion Rate of TiO_2 Film Electrode Surfaces by Anodic Polarization, J. Phys. Chem. B, 105 (2001) 3023-3026.

[39] N. Stevens, C. I. Priest, R. Sedev, J. Ralston, Wettability of Photoresponsive Titanium Dioxide Surfaces, Langmuir, 2003, 19, 3272-3275.

FIGURE CAPTIONS

Fig. 1. Current transients of titanium during anodizing at 3 V (MP-3V) and 20V (MP-20V) in 0.6 mol dm^{-3} K_2HPO_4 + 0.2 mol dm^{-3} K_3PO_4 glycerol electrolytes containing 0.03 mass% water at 433 K for 3.6 ks.

Fig. 2. Scanning electron micrographs of fractured cross-sections of the (a) MP-3V and (b) MP-20V specimens formed by anodizing for 3.6 ks. The insets are low magnification images of the cross-sections.

Fig. 3. Pore size distributions in the MP-3V and MP-20V specimens with 5 μm-thick anodic films. The distributions were obtained from nitrogen adsorption isotherms at 77 K.

Fig. 4. GDOES depth profiles of the (a) MP-3V and (b) MP-20V with 5 μm-thick anodic films.

Fig. 5. X-ray diffraction patterns of the MP-3V and MP-20V specimens, together with the NT specimen annealed at 723 K in air for 3 h. Each film thickness is 5 μm.

Fig. 6. (a), (b) Transmission electron micrograph of ultramicrotomed sections of the MP-20V specimen and (c) Selected area electron diffraction patterns taken from the anodic films. The areas enclosed by white lines in (b) show the crystalline nanograins.

Fig. 7. Cyclic voltammograms of the MP-3V and MP-20V specimens, together with the NT specimen annealed at 723 K in air for 3 h. Each film thickness is 5 μm.

Fig. 8. Comparison of photocatalytic decomposition rates of methylene blue for the MP-3V and MP-20V specimens, together with the NT annealed at 723 K in air for 3 h. Each film thickness is 5 μm.

Fig. 9. Contact angle of the MP-3V and MP-20V specimens, together with the NT specimen annealed at 723 K in air for 3 h as a function of UV-irradiation time.

Table 1. BET roughness factor of MP-3V and MP-20V specimens, together with the NT specimen annealed at 723 K in air for 3 h. Each film thickness is 5 μm.

Sample	**MP-3V**	**MP-20V**	**NT**
Roughness factor	1314	650	174

Table 1. Y. Taguchi, et. al.

List of Figures

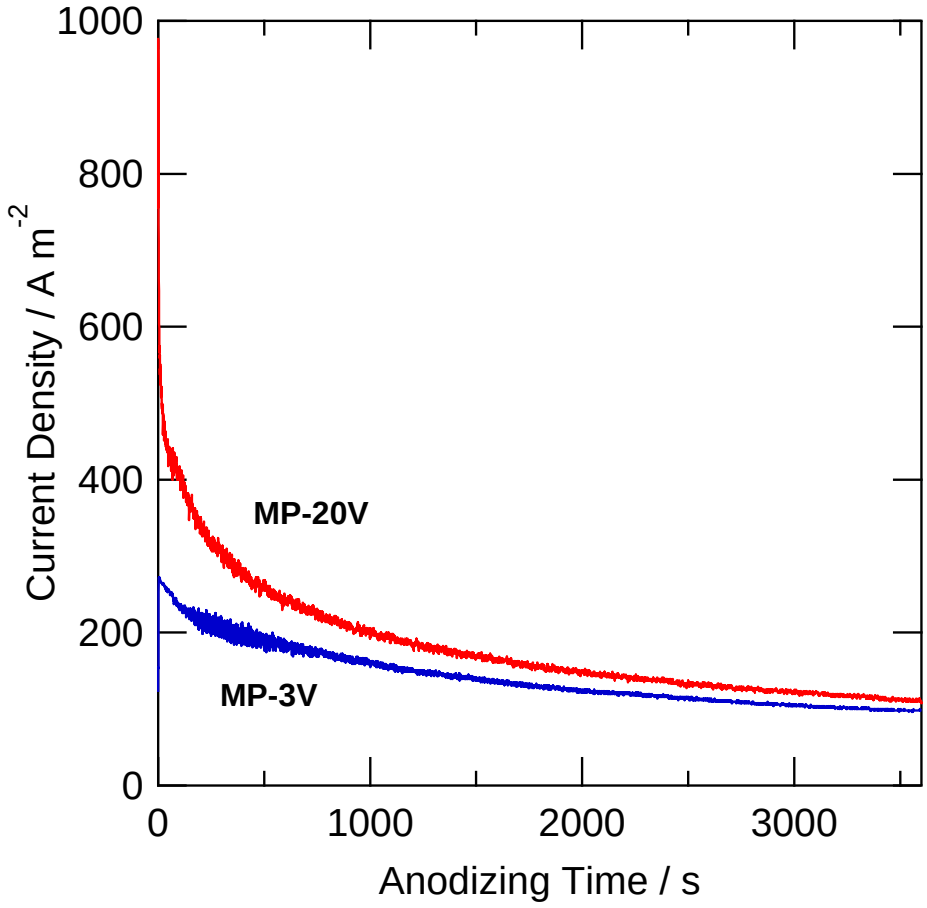

Fig. 1. Y. Taguchi, et. al.

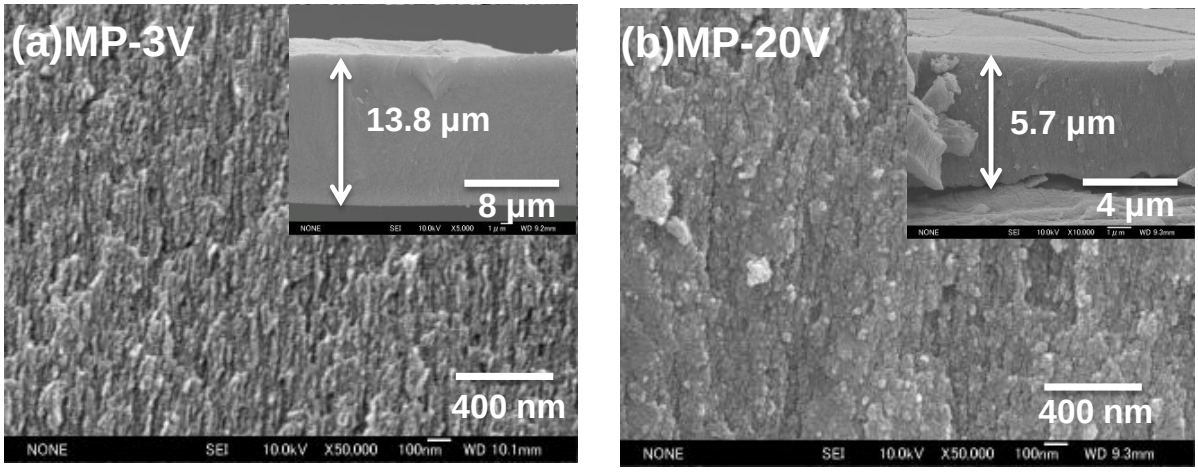

Fig. 2. Y. Taguchi, et. al.

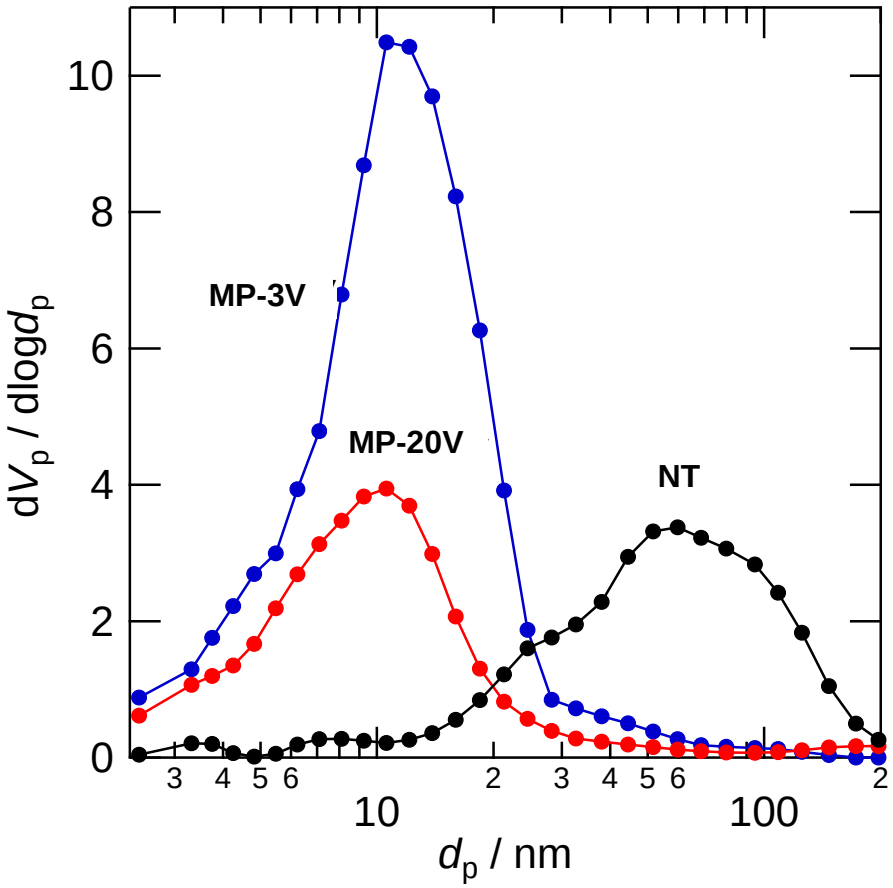

Fig. 3. Y. Taguchi, et. al.

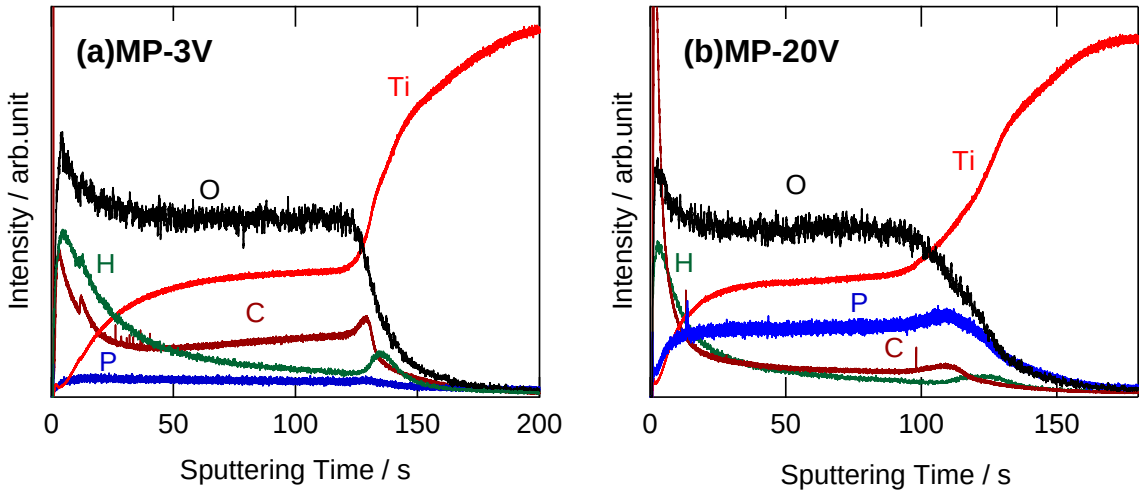

Fig. 4. Y. Taguchi, et. al.

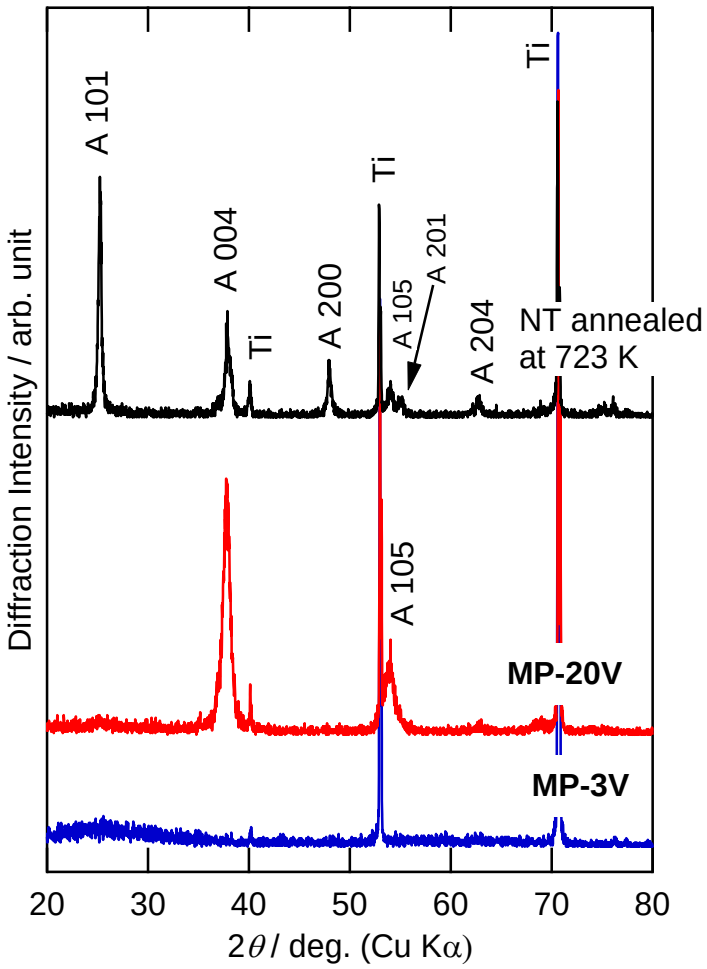

Fig. 5. Y. Taguchi, et. al.

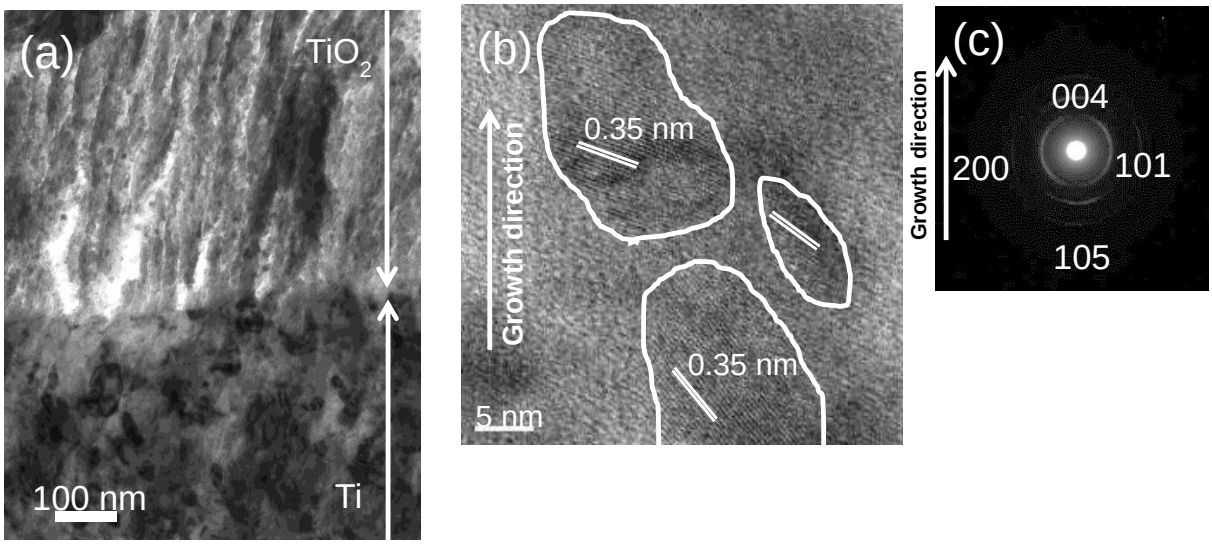

Fig. 6. Y. Taguchi, et. al.

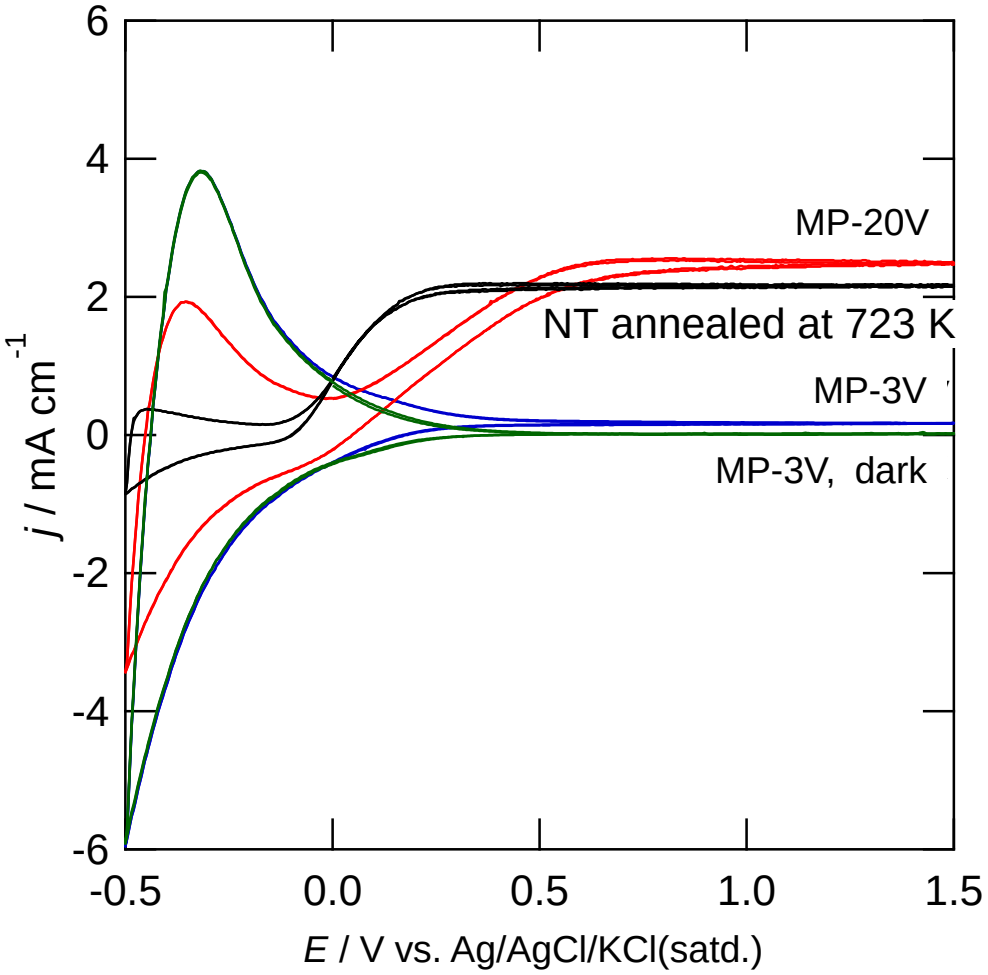

Fig. 7. Y. Taguchi, et. al.

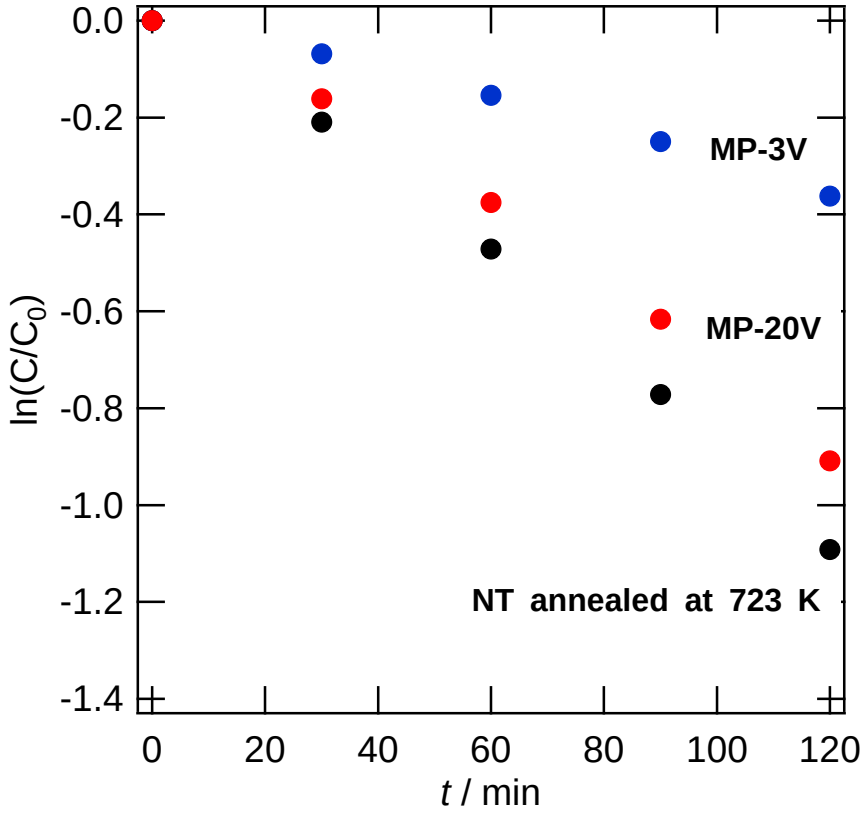

Fig. 8. Y. Taguchi, et. al.

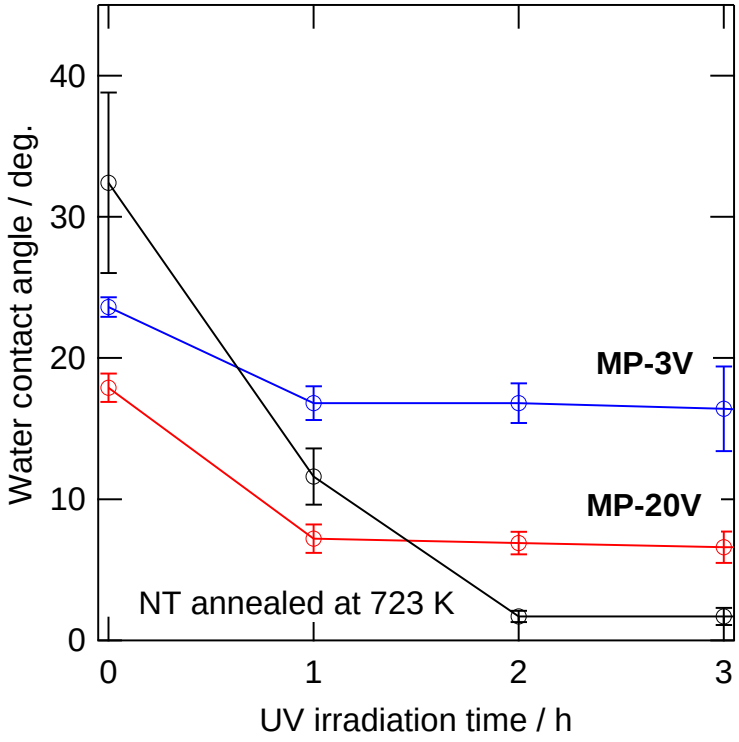

Fig. 9. Y. Taguchi, et. al.